Impact of extratropical cyclone intensity and speed on the extreme wave trends in the Atlantic Ocean

Carolina B. Gramcianinov[1*†], Ricardo de Camargo[1], Ricardo M. Campos[2,3], Carlos Guedes Soares[4], and Pedro L. da Silva Dias[1]

[1]Departamento de Ciências Atmosféricas, Instituto de Astronomia, Geofísica e Ciências Atmosféricas, Universidade de São Paulo, Rua do Matão 1226, Cidade Universitária, São Paulo, SP, Brasil

[2]Cooperative Institute for Marine and Atmospheric Studies, University of Miami, 4600 Rickenbacker Causeway, Miami, 33149, Florida, USA

[3]Atlantic Oceanographic and Meteorological Laboratory, NOAA, 4301 Rickenbacker Causeway, Key Biscayne, 33149, Florida, USA

[4]Centre for Marine Technology and Ocean Engineering (CENTEC), Instituto Superior Técnico, Universidade de Lisboa. Rovisco Pais, 1049-001 Lisboa, Portugal

*Corresponding author(s). E-mail(s): carolina.gramcianinov@alumni.usp.br

Contributing authors: ricamarg@usp.br; ricardo.campos@noaa.gov; c.guedes.soares@centec.tecnico.ulisboa.pt; pedro.dias@iag.usp.br

†Currently at Institute for Coastal Systems Analysis and Modeling, Helmholtz-Zentrum Hereon, Max-Planck-Straße 1, Geesthacht, 21502, Germany

For publication in

Climate Dynamics

Abstract

This work analyzes the extratropical cyclone-related extreme waves in the ocean surface and their trends in the North and South Atlantic Oceans. Atmospheric and ocean wave products are obtained from ERA5, from 1979 to 2020 with 1-hourly outputs, covering 42 years with the present climate changes evaluated by the difference between the two 21-years-time slices. The cyclones are tracked through the relative vorticity at 850 hPa and then associated with extreme wave events using an automated scheme that searches for an extreme wave region 1500 km from the centre of the cyclone, following criteria that exclude possible swell dominated events. The hot-spot regions of cyclone-related waves occurrence found by the method are in agreement with previous studies and are related to the cyclogenesis region and storm track orientation. Most cyclones associated with extreme wave events are generated in the western boundary of the domains. The east-poleward side of the ocean basins presents the highest density of occurrences related to the higher density of cyclone track and the dominance of more mature stage cyclones while in the west side prevail systems on developing stages, with notable propagating fronts and consequently, lower wind persistence. The storm track variations alone cannot explain the observed changes in the wave occurrence during the period due to the lack of statistical confidence. However, the wave occurrence responds to changes in the cyclone intensity, modulated by cyclone displacement speed. Regions with an increase of extreme waves are related to the effect of more intense cyclones or cyclones with slower propagation, being the last associated with a longer interaction of winds with the ocean surface.

1 Introduction

In the last decades, the demand to access changes on extreme events has been increasing. From an ocean perspective, the study of natural hazards associated with anomalous wind-generated ocean waves (hereafter only waves) is of paramount importance to offshore and coastal activities, with high socioeconomic impacts. Management and maintenance of ships, offshore and coastal structures depend upon knowing the current extreme wave climate and its trends (Bitner-Gregersen et al, 2018; Bernardino et al, 2021). In mid to high latitudes, the main drivers of wave climate are the extratropical cyclones, which are known by their strong winds and large fetch (e.g., da Rocha et al, 2004; Ponce de Léon and Guedes Soares, 2014, 2015;

Campos et al, 2018; Ponce de Léon and Bettencourt, 2021). In this context, this present study explores the relation between the extreme wave climate and extratropical storm tracks in the Atlantic Ocean, providing a new perspective of the changes in the extreme wave events forced by these atmospheric systems.

One of the challenges regarding wave climate trends studies is that wave distribution cannot be directly related to wind changes. The global wave climate is characterized by large waves in high latitudes, presenting a decrease in significant wave height (swh) towards the equator (Young, 1999). This distribution places the westerly wind belt, which generally indicates the preferred pathway of extratropical cyclones displacement (so-called storm track), as a wave generator in which waves are fully coupled with the overlayer winds (Chen et al, 2002) in a state known as wind-sea. After leaving their generation region, these waves can travel far distances and are able to cross ocean basins with low energy attenuation (Alves, 2006; Ardhuin et al, 2009). Such propagating waves are called swell, which combined with the wind-sea results in combined sea states (Guedes Soares, 1984; Vettor and Guedes Soares, 2020). Thus, changes in wave climate are not a straightforward response of the local winds (e.g., Stopa and Cheung, 2014). One solution to evaluate the wind-wave climate relationship would be separating local from remote forcing waves; however, it is not a trivial effort, especially in regions with high influence of swell and wind-sea (Rapizo et al, 2015).

Another problem is the varying range of influence that the cyclone structure (i.e., front positions and movement), displacement speed, and intensity play on the extreme wave occurrence. Even though climate state is a result of the average of weather patterns, changes in the extreme climate must be analysed with more caution regarding special conditions that lead to extreme events. For instance, within the extratropical wind structure, different patterns can generate extreme waves depending on the dominant air-flow. Bell et al (2017) found the influence of both cold and warm conveyor belts in the extreme waves in the Northern Sea while Kita et al (2018) reported extreme waves in distinct portions of the cyclones, such as along the warm front. These studies showed that beyond the climatological pattern, extreme wave studies also need to focus on the characteristics of the generating systems (i.e., the cyclone itself, as well as the sectors with stronger surface winds).

There are several studies about trends and changes of storm tracks in the current climate century (Simmonds and Keay, 2000;

Fyfe, 2003; Wang et al, 2006) and future scenarios (e.g., Ulbrich et al, 2009; Catto et al, 2019) but without a direct relation with waves. Globally, the storm track is shifting poleward, resulting in an overall decrease of cyclones at mid-latitudes (e.g., Fyfe, 2003; Geng and Sugi, 2003). However the change signal varies locally, and some regions may present an increase of cyclogenesis, such as the southwest South Atlantic coast, between 35°S and 40°S (Reboita et al, 2018, 2020). Regarding cyclone intensity, some studies showed the increase in the occurrence of strong cyclones, considering different intensity measurements for both the current climate (Pezza and Ambrizzi, 2003; Reboita et al, 2015) and future scenarios (Geng and Sugi, 2003; Lambert and Fyfe, 2006; Bengtsson et al, 2009). Moreover, Reboita et al (2021) found an increase of 13% in the occurrence of bomb cyclones in the South Atlantic Ocean, with the worst projected scenario (RCP8.5) presenting deeper, faster and shorter systems. An extratropical cyclone is called an explosive or bomb when it experiences fast deepening over a relatively short time, usually greater than 24 hPa in 24 hours (normalized at 60°N, Sanders and Gyakum, 1980). A significant positive trend of bomb cyclones in the Southern Hemisphere (SH) was also reported by Lim and Simmonds (2002) analysing the NCEP2 product from 1979 to 1999.

These findings allow a glance at what may happen with wave fields but the extreme wave climate may not be exclusively related to cyclone intensity or storm track location. First, because of the remote partition of the wave climate, as explained above, and secondly, because some cyclones simply do not generate extreme waves. Gramcianinov et al (2021b) showed that around 60% of the extratropical cyclones in ERA5 are associated with swh higher than 5 m in the Atlantic Ocean. Other factors, such as cyclone displacement speed and fetch orientation, play a big role in extreme wave generation and need to be taken into account in trends and changes studies (Gramcianinov et al, 2021a).

Some recent studies faced difficulties to explain wave trends just by using winds or storm track tendencies. According to Young and Ribal (2019), who evaluated the global trends of wind and waves through three satellite datasets between 1985 and 2018, the wind speed distribution is broadening, with an increase in the mean, mode and percentiles, but this behaviour is not followed by the wave height distribution. The authors found a tendency of higher occurrences of small waves, resulting in a distribution skewed to the left and the increase in 90^{th} percentile waves is confined to the

Southern Ocean and North Atlantic Ocean. Moreover, Takbash and Young (2020) found a positive tendency in wave height extremes in the SH, presenting an increase in the centennial swh (swh_{100}) of up to 3 cm/year using ERA5. The Northern Hemispheric trend was negative, but generally not statistically significant. In general most of the studies have shown an increase in wave height extremes in the SH in the past 41 years and that this is projected to continue in the future (e.g., Dobrynin et al, 2012; Lemos et al, 2019).

The present work applies a cyclone feature-based analysis (Lagrangian) to relate this extratropical system to extreme wave events in the Atlantic Ocean. Each cyclone associated with an extreme event is selected to build a set of statistical analyses regarding the cyclone-wave characteristics. The main goal is to investigate the trends in the cyclone-related waves, building a climatology of these extreme events for the last 42 years. This article is guided by three main questions: (1) What is the distribution of extratropical cyclones that most affect the extreme wave climate in the Atlantic Ocean?; (2) Which are the main characteristics of these cyclone-related waves?; and (3) Are there some significant trends in the storm track and wave events in the last decades?

The document presents a description of datasets and methods used in Section 2, including the key procedures of extreme wave definition and its association with cyclones. Section 3 shows the results, which are discussed in Section 4. Finally, the conclusion and recommendations are made in Section 5.

2 Data and Methods

2.1 ERA5

ERA5 is the fifth generation of reanalysis from the European Centre for Medium-Range Weather Forecast (ECMWF; Hersbach et al, 2020), produced with the ECMWF's Integrated Forecast System (IFS), version CY41R2, using 4D-Var data assimilation. The atmospheric and wave variables used in this work are on 0.28° and 0.36° horizontal grids, respectively. The data were used with 1-hourly outputs from 1979 to 2020 and obtained through the Copernicus Climate Change Service (C3S) (2017).

ERA5 presents several improvements regarding its predecessor, the ERAInterim, including development in model physics, core dynamics and data assimilation. Using ASCAT observation as a

reference, Belmonte Rivas and Stoffelen (2019) showed that ERA5 surface winds present a 20% improvement relative to ERA-Interim. Gramcianinov et al (2020a) compared the Atlantic Ocean's storm track characteristics for ERA5 and CFSR/CFSv2 from 1979 to 2019. These authors found that despite both datasets presenting cyclones' climatology in agreement with past studies, the 1-hourly ERA5 produces more continuous track and fewer tracking issues in continental and coastal regions. Considering the wave parameters, Takbash and Young (2020) analysed the magnitude and spatial distribution of mean and extreme wave parameters and found that ERA5 presents a good agreement with estimations from altimeter and buoy data. Further information about the main characteristics of ERA5 and a comparison with ERA-Interim can be found in Hersbach et al (2020).

2.2 Cyclones dataset

The cyclone tracks are obtained from the "Atlantic extratropical cyclone tracks database" (AETC) available at Gramcianinov et al (2020b). The AETC uses the TRACK program (Hodges, 1994, 1995, 1999) to identify and track the cyclones, following the method described in Hoskins and Hodges (2002, 2005). A detailed explanation of the method, tracking setup, and evaluation can be found in Gramcianinov et al (2020a), although some relevant details are given in this section. The AETC tracks produced using 1-hourly ERA5 fields are used in this study. CFSR and ERA5 present similar storm track spatial patterns and characteristics, but the use of hourly fields may produce broken tracks to CFSR.

The cyclonic features are identified using the relative vorticity at 850 hPa, which is recommended for the detection of cyclones in middle latitudes (Sinclair, 1994). Mid-latitude strong surface pressure gradient usually masks cyclones, therefore, hindering their detection when using mean sea level pressure (MSLP) fields for the tracking. The target systems are mainly extratropical cyclones, retained by a spectral filter applied during the pre-processing steps. Some subtropical systems can be retained as well, depending on their size. However, in this work, no distinction is made between these two types of systems as the interest is in any cyclone that can generate extreme waves in the extratropical region. AETC includes cyclones that last at least 24 hours, travel further than 1000 km, and pass within the extratropical latitudes of the South Atlantic (85°S-

25°S, 75°W-20°E) and North Atlantic (85°N-25°N, 65°W-0°E) at any moment of their lifecycle.

2.3 Extreme wave definition

The definition of an extreme relies on a threshold that can be established either by fixed values or percentiles. In this work, extreme percentiles are used to select wave events by applying a spatial approach adapted from Gramcianinov et al (2020c). The 90^{th}, 95^{th}, and 99^{th} percentiles are obtained through the distribution of the maximum swh of each event in the time series for each grid point. The definition of a time window is essential to guarantee the independence of each swh peak. To simplify the procedure to use for a large domain a fixed time window is adopted. Several authors used 48 h (e.g., Caires and Sterl, 2005; Meucci et al, 2020), but to short time windows tend to bias the percentiles in subtropical latitudes since in this location the frequency of systems is smaller. Tests on finding a suitable time window were made, following the autocorrelation method applied by Gramcianinov et al (2020c), resulting in the value of 96 h. In this way, the peaks used for the maximum swh distribution are selected considering a minimal interval of 96 h between the peaks. The extreme percentiles obtained for the North and South Atlantic basins in the summer and winter can be found in Fig. A1 and A2 of the Supplementary Material.

After selecting the percentiles, the points above the threshold in each time frame are grouped into regions that are afterwards associated with a cyclone track. The centre of mass of each extreme wave region is used in the search and connection with the cyclone centre. The method requires some adaptation from the original one since its application to a larger domain can result in a spurious association between cyclones and extreme waves. Three assumptions are made to restrict the association and to guarantee that the extreme wave is influenced by the local wind, as indicated hereafter.

1. The extreme event is associated with the cyclone that exists at least 1 day before the extreme region. This criterion is important to avoid the association of secondary cyclones to the wave extremes generated by a parental cyclone - considering that waves need a time scale of days to develop even for the highest wind speeds (Hasselmann et al, 1973; Ardhuin and Orfila, 2018).

2. To avoid the inclusion of swell dominated extremes consideration is given to extreme points in which the significant height of wind waves (shww, given by ERA5) corresponds to more than 50% of the swh. While the swh is calculated using the integral over all two-dimensional wave spectrum, the shww uses only the wind-sea wave spectrum obtained by only considering the components of the two-dimensional wave spectrum that are still under the influence of the local wind. Separating swell from wind-sea is not trivial, especially in a high wave generation environment such as the Southern Ocean (Rapizo et al, 2015), which is partially covered by the present domain. Other approaches, such as establishing a minimum value for the difference between wind and peak wave direction (e.g., 90° by Rapizo et al, 2015) it is not practicable in such a high-resolution grid. Interaction between remote propagating and local waves can remain, but focusing on extreme percentiles also helps the exclusion of swell dominated cases.
3. The cyclone centre is associated only if it is within 1500 km from the centre of mass of the extreme wave region. The cyclone-related waves are then defined in this work as an extreme wave region associated with a local cyclone by the method described above.

2.4 Cyclone-related wave parameters

Several cyclone parameters are calculated using the track information provided by the AETC dataset. The maximum 10-m wind speed is added to each track by a general search for the maximum value within a 6° radius of the cyclone centre (Bengtsson et al, 2009) and is used as a measure of cyclone intensity together with the vorticity. The centre of the cyclone along the track is also used to calculate cyclone displacement and the distance and the relative position between cyclone and extreme wave regions. The entire track information of the cyclone is used to produce the storm track statistics.

Mean parameters of the cyclone-related waves are used to compute statistics, producing distribution maps of mean swh (swh_{mean}), maximum swh (swh_{max}), mean wave direction, mean 10-m wind direction, and others. These parameters are obtained directly from the ERA5 products and the value associated with each case is

the average between all points in the extreme regions (i.e., that overpasses the extreme percentile).

Spatial statistics of cyclone-related wave parameters, cyclone genesis and track distribution are computed using the spherical kernel estimator approach (Hodges, 1996). The maps are built using the position of the centre of mass of the extreme wave region while the cyclone spatial statistics uses the centre of the cyclones. The tendencies are calculated through differences between the two 21 years' time slices in the whole period and were tested using the Monte Carlo significance test (Hodges, 2008) with 1000 samples of the set of tracks for each period.

The results focus on the winter and summer for each basin once they represent two opposite states in the annual cycle. To the North Atlantic analysis, the boreal summer is defined as June, July, and August (JJA) and the winter as December, January, and February (DJF). To the South Atlantic, the austral summer and winter are defined as DJF and JJA, respectively.

3 Results

3.1 Extreme wave events

The cyclone-related extreme wave distribution obtained based on different percentiles is presented in terms of density in Figs. 1 and 2, which may be interpreted as the frequency in which a location (area = 5° spherical caps) is affected by extreme waves in a month, not distinguishing the same event along the time axis. This means that long events also contribute to high densities.

In the North Atlantic (Fig. 1), there are three hot spots for extreme wave events located on the northeastern USA coast, south of Greenland, and northwest of the British Islands. The last two regions are highlighted in all percentiles, however, the US coast becomes more evident in more extreme thresholds (Fig. 1c-f), in both seasons. The winter presents higher densities than the summer, especially in the hot spots further north. In the summer, the high density near the British Islands shifts slightly southward. One can note that the distribution of events is highly concentrated between 45°N and 70°N during the winter, despite the zonal maximum around 60°N. This pattern is a consequence of the large fetches produced by the extratropical winter storms between North America and Europe,

which is distinct from the wider spread events observed in the South Atlantic (Fig. 2).

The South Atlantic presents a more zonal distributed event occurrence (Fig. 2), with a high density between 40°S and 55°S and similar densities range in both seasons, even though the summer presents slightly less event occurrence. The Drake Passage (DKP) and its surroundings, in the eastern boundary of the domain, present higher densities in all percentiles for both seasons. However, it is possible to note that the high density shifts southeastward with the increase of the percentile. This region is known for the high waves and bad navigation conditions (e.g., Campos et al, 2020). In the winter, the southwestern South Atlantic (swSA), between 50°S and 35°S along the South American coast, appears as a hotspot of events, which is more evident in the 99^{th} percentile. In fact, the swSA generally presents higher density than other locations at the same latitude, showing a density distribution skewed to the west, especially in the summer.

Cyclone-related wave events dominate the overall extreme wave distribution, being responsible for more than 65% of the events in most of the study domains (see Supplementary Figs. A3 and A4). The direct effect of cyclones in the wave climate increases according to the swh percentiles but is relatively small in the high-latitude and east-side of the ocean basins (e.g., Portugal and Morocco coasts in the NA and South African and Namibian coasts in the SA). An important remark is that is difficult to estimate how much cyclone-generated waves account for swh field, i.e., in the swh percentiles, due to the superposing of wind-sea and swell. Even trying to separate our events from swell dominated events during the cyclone-related event selection, superposing still exists in some cases. However, it is possible to see that regions reported to be swell dominant appear with a low percentage (< 60%) of cyclone-related wave events, such as the coast of Portugal, Greenland, Brazil, and South Africa.

3.2 Cyclones associated with extreme waves

Table 1 presents the annual mean of cyclones associated with extreme waves for each domain, season, and percentile. In the 1979-2020 period, the NA presented 38 and 17.5 cyclones per year related to the 90^{th} percentile wave occurrence, for the boreal winter (DJF) and summer, respectively, which corresponds to 24.4% and 14.9% of the cyclones in these seasons. The percentages of wave-associated cyclones follow the reduction of the cyclones in more extreme

percentiles, with almost double the cyclones in the winter than in the summer. In the SA, differences between the austral summer (DJF) and winter (JJA) are not so evident. Between 1979 and 2020, the SA presented 32.5 and 39.2 associated cyclones per year for the summer and winter, considering the 90^{th} percentile waves. The percentage of associated cyclones in the summer is slightly larger than in the winter, even though the former presents a lower annual mean.

Cyclone genesis and track densities computed for the cyclones associated with extreme waves are presented in Fig. 3 and 4 for the North Atlantic and South Atlantic, respectively. In the North Atlantic, the genesis densities show three main genesis regions: lee of the southern Rockies Mountains (35°N, 102.5°W; RKM), USA northeastern coast (40°N, 75°W, USC), and Central East Atlantic (centred at 55°N, 30°W, CEA). North Atlantic storm track climatologies (Dacre and Gray, 2009; Hoskins and Hodges, 2002, 2019) have reported four regions, adding the high occurrence of cyclogenesis on the eastern coast of Greenland, which is less relevant to cyclone-related waves according to Fig. 3. The cyclonic activity in the North Atlantic is more intense in the boreal winter (DJF), which reflects in the climatological genesis and track densities distribution. In the winter, the three genesis regions are present while only RKM and USC are relevant during the summer.

Regarding the percentiles, the USC gains even more relevance with the increase of percentile when compared to the other regions. The North Atlantic storm track presents a northeast orientation across the basin (e.g., Hoskins and Hodges, 2002; Gramcianinov et al, 2020a), which is also reproduced by the selected cyclones (Fig. 3). Two regions present high track density and their importance changes according to the season and percentile. During the winter, there is a main storm track along the northeastern USA coast, followed by a secondary branch in the Northeast North Atlantic (NNA). The secondary storm track loses its signal in higher percentiles, indicating that a big part of the cyclones associated with extreme events in the basin comes through the USA coast in this season. The summer has a dispersed and weak storm track but the large densities occur poleward, covering the NNA region.

In the South Atlantic (Fig. 4), the cyclogenesis concentrates along the South American south and central coast, following the three main genesis regions reported by the literature (e.g., Hoskins and Hodges, 2005; Gramcianinov et al, 2019, 2020a). In the austral winter (JJA), the genesis region around 30°S in La Plata Basin (LPB) are more

active, but the genesis over Argentina (ARG) is usually the largest over the whole year. However, the genesis density in the LPB region overpasses the ARG region in the higher percentiles (Fig. 4d, f). These two genesis regions also appear in the summer densities distribution, with the ARG genesis activity leading in all percentiles. Moreover, in the 90^{th} percentile (Fig. 4a) a genesis density higher than 1 cyclone per season appears covering a region up to 25°S, along the Southeast Brazilian coast (SBR), which is usually associated with subtropical cyclogenesis and transitions (Gozzo et al, 2014; da Rocha et al, 2019; de Jesus et al, 2020). The track density reflects the genesis density, showing the displacement of the cyclone eastward with a slight tilt poleward, a typical characteristic of the South Atlantic's storm track (Hoskins and Hodges, 2005). However, when comparing to the climatology (Gramcianinov et al, 2020a), it is possible to see that the subtropical path of the storm track is more evident in Fig. 4, due to the large relevance of cyclones generated at LPB and SBR associated with the extreme wave climate.

The intensity and speed distribution of the cyclones associated with extremes are presented as their deviation from the climatology for the same period in Fig. 5. Due to similarity, only the results for the 90^{th} are presented. The cyclones associated with extreme waves are more intense regarding the wind speed at 10-m (Fig. 5a-d). The distribution of this intensification follows the storm track behaviour, reaching lower latitudes in the winter when the cyclone track density is spread. These cyclones are generally slower than climatology as is possible to see by the dominance of negative values in Fig. 5e-g. The speed difference is smaller and can be even positive in the main storm track position where the upper-level jet is stronger, driving the cyclone propagation.

3.3 Cyclone-related waves characteristics

The spatial distributions of cyclone-related waves characteristics were analyzed only for the 90^{th} (Fig. 6 and 7) due to the similarity with the other percentiles. Moreover, the 90^{th} percentile was selected because the higher number of cases in this percentile allows more robust estimations of the spatial patterns and trends (Section 3.4).

The swh_{mean} and swh_{max} associated with the cyclones (Fig. 6) follow the climatological pattern of both basins, with smaller values equatorward (Young, 1999; Vinoth and Young, 2011). The exception is in the North Atlantic for the summer (JJA, Fig. 6b,f), which presents

slightly high values westward of the domain, probably due to the influence of USC cyclones (Fig. 3). Despite that, for NA winter (DJF) and SA, both swh_{mean} and swhmax follow the orientation of the storm track (Figs. 3 and 4), with the large values poleward in the middle-east side of the domains, overlapping the downwind of the storm track (Ponce de Léon and Bettencourt, 2021).

The mean wave direction of the events (Fig. 7a-d) presents a prevalence of W (240°-300°) and SW (210°-240°) waves in the major part of the NA and SA. In the NA (Fig. 7a, b), extreme events with mean wave direction from S (150°-210°), SE (120°-150°), and E (60°-120°) occur in the USC and Greenland's surroundings, especially in the summer (JJA). Around 35°N, near the Portuguese and North Africa coast, the cyclone-related mean wave direction changes from W in the winter (DJF) to S and SE in the summer (JJA). Seasonal variability of the mean wave direction of the cases is also observed in the SA (Fig. 7c,d), where it is possible to find extreme waves propagating from S and SW in the Argentina, Uruguay, and Southern Brazil coasts and SE and E in the SBR. The mean 10-m wind direction distributions associated with the cyclone-related waves present the same pattern and can be found in Fig. A5 of the Supplementary Material.

Regarding the cyclone sector where the wave extreme occurs (Fig. 7e-h), one can observe that in the NA, most of the events in mid-latitudes occur in the S, SW sector of the cyclone, in agreement with the dominant wave and wind mean direction (Fig. 7e,f). In mature and early-occlusion stages, typical of the mid-Atlantic and NNA storm track, this sector of the cyclone is dominated by the cold conveyor belt, located behind the cold front. In the SA (Fig. 7g, h), the analogous situation is observed with the wave extremes occurring mainly in the W and NW sector of the cyclone. However, a comment may be made in the SBR region during the summer (DJF), where the extreme events occur mainly in the E sector of the cyclone with the mean wave direction from E and SE, which indicate the influence of the warm conveyor belt in this location, as observed by Gramcianinov et al (2020c). Along the Southern Brazilian coast, but in winter, the dominant sector is W/NW, with the mean wave direction and 10-m wind direction from S and SW, in agreement with Gramcianinov et al (2021a). According to these authors, yet during the winter, there is a prevalence of the cold conveyor belt in early to mature-stage cyclones, and the extreme waves occurred in the downwind of the cyclone fetch along the coast.

3.4 Changes in 42 years of reanalysis

Considering the annual means presented in Table 1 for the two 21-yr time slices, it is noticeable a slight increase or decrease in cyclone number associated with extreme waves, depending on the season. However, the changes are not significant compared to the standard deviation of the annual mean. NA presents an increase in the associated cyclones in the boreal winter (DJF) in the 90^{th} and 95^{th} percentiles, but a decrease in the 99^{th}. In the summer (JJA) the increase occurs in the 95^{th} and 99^{th} percentiles. In the austral winter (JJA), SA also presents an increase in the cyclones associated with the 90^{th} and 95^{th} percentiles waves, with a decrease in the higher percentile. However, in the summer (DJF) there is a general increase of associated cyclones in all percentiles for the SA.

Figures 8 and 9 present the trends in the cyclone-related wave occurrence, representing the changes between the two 21-yr time slices, for the NA and SA. The tendency of the 99^{th} percentile is not presented due to the lack of statistical confidence, as explained in the last section. In general, the trends are very heterogeneous within the domains and between summer and winter. Moreover, although the signal pattern is mostly similar between the extreme percentiles, its relative importance varies depending on the percentile.

North Atlantic winter tendencies (DJF, Fig. 8a, c) show a decrease in the occurrence of extreme cyclone-related wave occurrence in the NNA, northward of Ireland and British Island. The region of high occurrence south of Greenland (Fig. 1) presents an eastward shift, with the events affecting more the eastern coast of the country. Offshore of the northeastern coast of the USA there is an increase in the occurrence of these events. There is also a slight increase of events in a band that overlaps North of Spain and Portugal but only in the 90^{th} percentile. The 95^{th} cyclone-related wave occurrence presents a decrease in this region. A very different pattern can be found in the summer (JJA, Fig. 8b,d), where an increase in the occurrence of events over the NNA is noted, covering not only the north but also the west sea offshore Ireland and British Island. The eastward shift of the occurrence hot-spot in Greenland is also observed, as well in the north of Spain. For the summer, there is a weak decrease of events on the northeastern USA coast.

Relative changes in the occurrence of cyclone-related waves are smaller in the SA, but interesting patterns can be observed. In the summer (DJF, Fig. 9a,c) most of the domain presents an increase in the occurrence of events, highlighting the region offshore South

American coast, from 50°S to 20°S, the region nearby Drake Passage, and between 45°S and 55°S in the southeast of SA. The South African coast presents a small but significant decrease in event densities. For the winter (JJA, 9b, d) changes, there is still an increase in the South American coast, but from 50°S to 40°S and only for the 90^{th} percentile. Between 40°S and 20°S, offshore Brazilian coast, there is a decrease in the event density. The east portion of the Drake Passage also presents an increase, but smaller than in the summer. African coast, between 30°S and 20°S, present a significant increase of cases.

The cyclone track density changes show an overall poleward increase in the storm track associated with extreme waves (Fig. 10 and 11), but with a lack of statistical significance. The differences are only significant in some points in the middle of the South Atlantic for the tracks based on the 90^{th} percentile (95^{th} percentile is not shown since it does not have any significant change). Despite that, the track changes are presented even to the NA to support further discussion about other changes in cyclone-related wave occurrence. In the NA (Fig. 10), the largest change occurs in the boreal winter (DJF), when the track density increases on the USA coast. In the summer (JJA), the NA storm track strength in the mid-to-eastern oceanic portion, which may be related to the increase in the cyclone-related wave density in the north portion of British Island. In the SA (Fig. 11), it is possible to observe a poleward shift of the associated cyclone tracks, similar to the reported general storm track behaviour in the last decades (e.g., Fyfe, 2003). However, in the SBR there is a slight increase in the cyclone track densities, probably indicating short duration cyclones with local effect.

Cyclone intensity based on the vorticity at 850 hPa and displacement speed changes have spatially heterogeneous distribution denoting the challenge of feature distribution analysis. NA (Fig. 10c, d) shows a slight increase in the cyclone intensity in mid-latitudes in the boreal winter (DJF), while in the summer (JJA) a general negative sign prevails, except by the western European coast. In the SA (Fig. 11c, d), the winter (JJA) presents an increase in the associated cyclones in the middle of the basin. In the summer (DJF) there is a decrease of intensity in the middle and eastern portion of the domain while it is possible to see an intensification in the SBR region. The cyclone speed increases present an increase in the NA winter (DJF) in mid-latitudes near the western European coast and USC (Fig. 10e). In the summer (JJA) there is a significant slowdown of cyclones over the NNA region (Fig. 10f).

The SA cyclones associated with extreme waves present an increase in their displacement speed in the major part of the domain in both seasons (Fig. 11e, f), except between 30°S - 20°S in the western portion of the basin. The overall increase in the cyclone speed may be related to the intensification of upper-level jets reported in some studies (e.g., Reboita et al, 2018). An important remark is that cyclones move according to the upper-level circulation rather than the surface winds (e.g., Hoskins and Hodges, 2002, 2019), which reflects the difference between cyclone intensity and speed distribution maps. A cyclone embedded in the upper-level jet tends to move faster than detached cyclones.

4 Discussion

4.1 Extreme waves and the extratropical storm track

The cyclone-related waves, defined here as the extreme wave regions directly associated with cyclones, present well-defined occurrence hot spots and the observed seasonal variability can be related to the storm track shifts. The seasonal variability is stronger in the NA, with much more events in the boreal winter (DJF) than in the summer (JJA). In the two ocean basins the cyclones associated with the extreme waves are generated preferentially in the western boundary, where the orography and warm ocean currents support their development (e.g., Grise et al, 2013; Gramcianinov et al, 2019). These cyclones travel to the east tilting poleward promoting extreme waves along the storm track and mainly in its downwind end, as reported by past studies (e.g., Ponce de Léon and Bettencourt, 2021; Ponce de Léon and Guedes Soares, 2021).

During the cyclone early stages, its development and intensification processes affect the positions of the fronts depending on the relative dominance of different air fluxes within the cyclones (e.g., warm and cold conveyor belts).

In this way, despite the cyclonic activity surrounding genesis regions, the lack of directional persistence of the winds and limited fetch size results in less extreme waves in the western sector of the domain. On the other hand, on the eastern portion where mature cyclones prevail, already fully developed, travelling eastward with more stable fetches relative to the cyclone displacement. The large size, intensity and stable structure of these advanced-stage cyclones allow the development of a large fetch with more stabilized wind

direction when compared to the cyclogenetic regions (Fig. 7), resulting in higher waves (Fig. 6) and large occurrences of extremes in the eastern boundary of the domain, close to the exit of the storm track. The relation between the higher waves in the mid-eastern part of NA, the storm track and the large fetch provided by mature cyclones are in agreement with previous studies that established this location as wind-sea dominated (Stopa and Cheung, 2014) and highly influenced by extratropical cyclones (e.g., Ponce de Leon and Bettencourt, 2021). However, the north of the British Island, usually considered swell dominant due to the diminishing of the wind-swh correlation (Stopa and Cheung, 2014) and the presence of longer waves (Young, 1999), appears in the results as relevant to the cyclone-related wave climate, revealing also an important local forcing.

The mid-oceanic genesis regions reported by Dacre and Gray (2009) for the NA and Gramcianinov et al (2019) for the SA play little influence on extreme wave generation due to the lack of time interaction with ocean surface, reinforcing the importance of cyclone lifecycle stage to extreme wave generation. One important point in the SA is that the LPB genesis region, which is responsible for producing most of the cyclone-related waves in the austral winter (JJA), also plays a big role in the summer (DJF) events, even not being very active in this season (e.g., Gan and Rao, 1991; Crespo et al, 2021). Another cyclogenetic region associated with wave extreme is the SBR, which is active in the austral summer (DJF) and where subtropical genesis and transitions between cyclone types are reported (e.g., Gozzo et al, 2014; da Rocha et al, 2019). The relation of SBR and LPB genesis with cyclone-related extreme waves within the SA domain can be related to the development of slower and/or stronger cyclones in subtropical latitudes, with the influence of high humidity income and warmer Brazilian Current (e.g., Gozzo et al, 2017).

The cyclones associated with extreme wave events present higher intensity regarding the vorticity and 10-m wind speed (Fig. 4a-d). The direct relation between wind intensity is expected by the Hasselman relation, which shows that the wave growth directly correlates with the wind speed. The increase of swh is also time-dependent, and the strong winds alone are not sufficient to fully develop extreme waves. Thus, the cyclone speed displacement also appears as a valuable parameter in our results, particularly in the regions outside the westerly belts in both hemispheres. In this

location between 35°S and 20°S (SA) and 55°N and 70°N (NA) the cyclone's speed is generally smaller than the climatology (Fig. 4e-h), which affect the occurrence of the cyclone-related waves, either by producing higher waves or by elongating the duration of the events.

On average, extreme wave events tend to occur in the cold sector of the extratropical cyclone, to the westward of its centre, where it is located the cold conveyor belt. However, as mentioned before, the cyclone lifecycle stage may change this location according to the relative position of the cold and warm fronts. In regions nearby cyclogenesis, such as the swSA and USC, extreme waves can take place in the warm sector of the cyclone (eastern side, Fig. 7e-h), being influenced by the strong warm advection during the cyclone development. The relative importance of the cold and warm conveyor belt has been explored by previous works (Bell et al, 2017; Kita et al, 2018; Gramcianinov et al, 2020c; Ponce de Léon and Bettencourt, 2021) and it can lead to different perspectives of extreme wave generation within the extratropical cyclones. In agreement with Gramcianinov et al (2020c, 2021a), it is observed that the SBR presents a high influence of the warm conveyor belt in the summer (Fig. 7g), which may not generate waves that propagate towards the coast, but can severely influence the wave climate offshore, where there are oil exploitation and navigation activities.

4.2 Changes in the cyclone-related waves

The changes in the cyclone-related extreme wave occurrence cannot be fully explained by the storm track trends reflecting the complex mechanisms behind extreme wave climate patterns. The results showed a link between the changes in extreme wave occurrence and the cyclones characteristics, such as intensity and displacement speed; a summary of this relation is schematically presented in Fig. 12. The discussion of the changes are focused on the regions with high cyclone-related wave density (Fig. 1 and 2) and significant large changes (Fig. 8 and 9) according to the 90^{th} percentile analysis (significant results). In general, for both basins, there was an increase in the occurrence of extreme waves associated with cyclones, which is indicated by the changes in the number of cyclones (Table 1), storm track (Fig. 10a,b and 11a,b), and cyclone-related extreme waves (Fig. 8a,b and 9a,b), although the signal is not always statistically significant.

The NA present four regions of important changes in the cyclone-related extreme wave occurrence: eastern USA coast, Greenland,

north of the British Islands, and west European coast. Despite the inclusion of the storm track changes in this discussion, more focus has been given to other parameters since the track density differences between the periods were not significant at any point in the NA. In the boreal winter (DJF), the strengthening of the storm track at the Eastern US coast may affect the extreme wave occurrence in this region and east-northeastward, including the west European coast between 40°N and 50°N (Fig. 8a). The changes showed that the cyclones developing in the USC and acting within 35°N and 50°N became stronger as well, which led to more extreme waves despite the observed increase in the cyclone speed over these regions. Further north in the domain, the East Greenland coast and British Islands are affected by the slight increase of the secondary storm track (not statistically significant). However, the former region presents an increase in wave occurrence due to the increase in cyclone intensity while the latter has weaker cyclones, presenting a decrease. Besides the cyclone intensity regulation, the summer pattern (JJA) showed a new element which was the effect of the decrease in the cyclone speed to the extreme wave occurrence. In the eastern Greenland coast and British Islands the cyclone intensity decrease was counterbalanced by a decrease of the displacement speed, elongating the cyclone's wind interaction with the ocean surface.

The same pattern can be extended to the SA, with its western portion presenting this counterbalance between intensity and speed in the summer (DJF). In the SA four regions are highlighted with important changes: the Southern Brazilian coast, western SA, Drake Passage, and southeastern SA. Changes in the SA storm track are statistically significant between 40°S and 55°S, revealing an increase in the track density therein. The increase in the cyclonic activity in this band influences especially the Drake Passage and eastern portion of the domain, potentially increasing the extreme wave occurrence in these regions. The exception is the southeastern SA, where the extreme wave occurrence decreases due to the weakening of the cyclone acting in that region in the winter (JJA).

Besides the high amount of criteria used along this work to obtain robust results, some limitations must be held to the discussion above. The relations made between cyclone characteristics and extreme wave regions considered a distance of 10° to 5° between them. Despite the use of 1500 km (15°) to link these features, the previous analysis showed that the distance is still within 200 - 700 km radius

from the cyclone centre (Gramcianinov et al, 2021a), which allows the local interpretation of the results made in this work. However, the direct relation between the cyclone and wave distributions used can be set as a limitation of this work, since some fields present heterogeneous change signals, making challenging the interpretation (i.e., the scale of the change signal is smaller than 5°). To attenuate this problem, only some regions are discussed, highlighted by their significant signal, location, and extreme wave occurrence. Furthermore, it is important to remember that the method applied has removed the swell from the wave signal and the discussion considered only cyclone-related wave events, forced locally. Although some remote signals can still be retained, it is not dominant and does not influence the discussion.

The difference between the two 21-yr time slices is used in the present work as a proxy of the change within the entire period. However, it is not possible to conclude if the obtained signal is driven by climate change or differences in multi-decadal atmospheric oscillations. The global wave climate varies according to interannual climate variations and teleconnections in both hemispheres (Wang et al., 2008; Hemer et al., 2010; Godoi et al., 2020; Godoi and Torres Junior, 2020; Sasaki et al., 2021). With a time slice of ~ 20 years, shorter interannual time-scales variability, such El-Nino Southern Oscillation (ENSO) and even part of Southern Annular Mode (SAM) is expected to be excluded. However, long-term variabilities in decadal scales, such as North Atlantic Oscillation (NAO), and Atlantic Multidecadal Oscillation (AMO) may influence the changes reported here. Nevertheless, it is relevant to access these changes to have a better overview of what is happening in the present climate to improve the analysis of the possible future scenarios.

5 Conclusion

The feature-based analysis applied in this work gave new insights into cyclone related wave climate distribution and characteristics. The results confirm and reinforce the findings in many extreme wave climatology studies (e.g., Vinoth and Young, 2011) and cyclone-related studies in the North Atlantic Ocean (Takbash et al, 2019; Ponce de Léon and Bettencourt, 2021; Gramcianinov et al, 2021b) and South Atlantic Ocean (Gramcianinov et al, 2020c, 2021a). The novelty of the present work relies on the direct link between

cyclones and extreme wave events to add information and justify the observed distributions and trends of the extreme wave climate.

The hot-spot regions of cyclone-related waves occurrence resemble the locations that present high extreme statistics when using the traditional approach (i.e., extreme-value analyses, Vinoth and Young, 2011; Campos and Guedes Soares, 2016a,b; Campos et al, 2019; Takbash and Young, 2020), such as the downwind end of the storm track due to accumulation of cyclone related fetches and wind intensity. However, it is important to note that the western sector of both domains also presents relevant cases, associated with the intensification stages of cyclones. These cyclone-related waves occur close to cyclogenesis regions in the western boundary of the basins, affecting off eastern South American and USA coasts - where such investigation cannot be neglected once these locations have high socio-economic value.

The cyclone lifecycle phase has been shown to play a big role in the extreme wave occurrence and swh distributions. In the early stages, strong winds are expected due to the cyclone development processes having enough intensity to generate extreme waves. However, the movements of the fronts in this phase contribute to a fast change of wind direction compromising the fetch persistence. On the other hand, in the middle of the storm track, cyclones in mature stages prevail, combining intensity and a more stable structure to generate a large fetch. Besides, cyclones associated with extreme waves are more intense, as expected, and present slower displacement speed when compared to the climatology, promoting extreme waves not just by the wind intensity but also due to the longer time of interaction between this wind and the ocean surface.

Considering 42 years, the changes in the distribution of cyclone-related events and cyclones characteristics are linked in different ways, and they result not only from the storm track position but also from a combination of factors. It is expected that changes in the storm track orientation play a big role in the cyclone-related wave climate. However, the results do not present significant changes in the storm track in most of the domains. Instead, the balance between the cyclone speed and intensity dictated the extreme wave changes. The local increase in cyclone intensity leads to an increase in the wave extremes, but the decrease of intensity does not necessarily result in a decrease of the waves (Fig. 12). In this situation, the cyclone speed behaves as a modulator: if the cyclones are somewhere slower, they counterbalance the weakness by increasing

the time of interaction between wind and ocean surface, i.e., wind persistence, increasing or elongating extreme wave events.

Despite the relatively small changes in cyclone-related extreme waves (up to 7.5 occurrences per month per area), the impact on the ocean and coastal activities are considerable, especially considering the 42 years-time interval. The statistics based on individual events applied in this work provide valuable information to assess trends and future changes, giving more insights about changes in the weather systems rather than overall climate change patterns.

Acknowledgements. The authors acknowledge the anonymous reviewer, who helped us to improve this article. This work is part of the project "Extreme wind and wave modelling and statistics in the Atlantic Ocean" (EXWAV) funded by the S˜ao Paulo Research Foundation (FAPESP) grant #2018/08057-5 and by the Portuguese Foundation for Science and Technology (Funda¸c˜ao para a Ciˆencia e Tecnologia – FCT) under contract PTDC/EAM-OCE/31325/2017 RD0504. This work contributes to the Strategic Research Plan of the Centre for Marine Technology and Ocean Engineering (CENTEC), which is financed by the Portuguese Foundation for Science and Technology (Funda¸c˜ao para a Ciˆencia e Tecnologia - FCT) under contract UIDB/UIDP/00134/2020. C.B.G. holds a FAPESP postdoc scholarship grant #2020/01416-0. The authors would like to acknowledge the ECMWF for providing the atmospheric and wave data for the study, as well as Dr. Kevin Hodges for providing the TRACK code. The ERA5 products were generated using Copernicus Climate Change Service Information [2019]. This study used the high-performance computing resources of the SDumont supercomputer (http://sdumont.lncc.br), which is provided by the National Laboratory for Scientific Computing (LNCC/MCTI, Brazil).

Declarations

Funding. grant #2018/08057-5, S˜ao Paulo Research Foundation (FAPESP); grant #2020/01416-0, S˜ao Paulo Research Foundation (FAPESP); contract PTDC/EAM-OCE/31325/2017, Fundac¸˜ao para a Ci ̂encia e Tecnologia - FCT; contract UIDB/UIDP/00134/2020, Funda¸c˜ao para a Ci ̂encia e Tecnologia FCT.

Availability of data and material. The ERA5 products were obtained with Copernicus Climate Change Service (C3S) (2017) (https://cds.climate.copernicus.eu/, last access: June 2021). The Cyclone tracks used in this study are available at "Atlantic extratropical cyclone tracks databases" (https://data.mendeley.com/datasets/kwcvfr52hp/5; Gramcianinov et al, 2020b). The cyclone track associated with extreme wave events obtained in this study can be shared upon request by email.

Code availability. The codes used in Section 3.3 can be shared upon request by email.

Authors' contribution. CBG: Conceptualization, Formal analysis, Methodology, Visualization, Writing — original draft. RC and RMC: Conceptualization, Methodology, Writing — review & editing. PLSD and CGS: Writing — review & editing, Supervision.

Conflict of interest. The authors declare that they have no conflict of interest.

References

Alves JHG (2006) Numerical modeling of ocean swell contributions to the global wind-wave climate. Ocean Model 11(1-2):98–122. https://doi.org/10. 1016/j.ocemod.2004.11.007

Ardhuin F, Orfila A (2018) Wind Waves. New Front Oper Oceanogr pp 393–422. https://doi.org/10.17125/gov2018.ch14

Ardhuin F, Chapron B, Collard F (2009) Observation of swell dissipation across oceans. Geophys Res Lett 36(6):1–5. https://doi.org/10.1029/ 2008GL037030, https://arxiv.org/abs/0809.2497

Bell RJ, Gray SL, Jones OP (2017) North Atlantic storm driving of extreme wave heights in the North Sea. J Geophys Res Ocean 122(4):3253–3268. https://doi.org/10.1002/2016JC012501

Belmonte Rivas M, Stoffelen A (2019) Characterizing ERA-Interim and ERA5 surface wind biases using ASCAT. Ocean Sci 15(3):831–852. https://doi. org/10.5194/os-15-831-2019

Bengtsson L, Hodges KI, Keenlyside N (2009) Will extratropical storms intensify in a warmer climate? J Clim 22(9):2276–2301. https://doi.org/10.1175/ 2008JCLI2678.1, https://arxiv.org/abs/9501047 [cond-mat]

Bernardino M, Gonc¸alves M, Guedes Soares C (2021) Marine climate projections toward the end of the twenty-first century in the North Atlantic. Journal of Offshore Mechanics and Arctic Engineering 143(6). https://doi. org/10.1115/1.4050698

Bitner-Gregersen EM, Vanem E, Gramstad O, et al (2018) Climate change and safe design of ship structures. Ocean Engineering 149:226–237. https: //doi.org/10.1016/j.oceaneng.2017.12.023

Caires S, Sterl A (2005) 100-year return value estimates for ocean wind speed and significant wave height from the ERA-40 data. J Clim 18(7):1032–1048. https://doi.org/10.1175/JCLI-3312.1

Campos RM, Guedes Soares C (2016a) Comparison and assessment of three wave hindcasts in the North Atlantic Ocean. Journal of Operational Oceanography 9(1):26–44. https://doi.org/10.1080/1755876x.2016.1200249

Campos RM, Guedes Soares C (2016b) Comparison of HIPOCAS and ERA wind and wave reanalyses in the North Atlantic Ocean. Ocean Engineering 112:320–334. https://doi.org/10.1016/j.oceaneng.2015.12.028

Campos RM, Alves JH, Guedes Soares C, et al (2018) Extreme wind-wave modeling and analysis in the South Atlantic ocean. Ocean Model 124(August 2017):75–93. https://doi.org/10.1016/j.ocemod.2018.02.002

Campos RM, Guedes Soares C, Alves JH, et al (2019) Regional long-term extreme wave analysis using hindcast data from the South Atlantic Ocean. Ocean Eng 179(March):202–212. https://doi.org/10.1016/j.oceaneng.2019. 03.023

Campos RM, D'Agostini A, Franc¸a BRL, et al (2020) Extreme Wind and Wave Predictability From Operational Forecasts at the Drake Passage. Journal of Offshore Mechanics and Arctic Engineering 143(2). https://doi.org/10. 1115/1.4048151

Catto JL, Ackerley D, Booth JF, et al (2019) The Future of Midlatitude Cyclones. Curr Clim Chang Reports 5(4):407–420. https://doi.org/10.1007/ s40641-019-00149-4

Chen G, Chapron B, Ezraty R, et al (2002) A global view of swell and wind sea climate in the ocean by satellite altimeter and scatterometer. J Atmos Ocean Technol 19(11):1849–1859. https://doi.org/10.1175/1520-0426(2002) 019h1849:AGVOSAi2.0.CO;2

Copernicus Climate Change Service (C3S) (2017) ERA5: Fifth generation of ECMWF atmospheric reanalyses of the global climate. Copernicus Climate Change Service Climate Data Store (CDS), URL https://cds.climate. copernicus.eu/cdsapp#!/home, last access: 20 Jan. 2021

Crespo NM, da Rocha RP, Sprenger M, et al (2021) A potential vorticity perspective on cyclogenesis over centre-eastern South America. International Journal of Climatology 41(1):663–678. https://doi.org/https://doi.org/10.1002/joc.6644

da Rocha RP, Reboita MS, Gozzo LF, et al (2019) Subtropical cyclones over the oceanic basins: a review. Ann N Y Acad Sci 1436(1):138–156. https://doi.org/10.1111/nyas.13927

Dacre HF, Gray SL (2009) The spatial distribution and evolution characteristics of North Atlantic cyclones. Mon Weather Rev 137(1):99–115. https://doi.org/10.1175/2008MWR2491.1

de Jesus EM, da Rocha RP, Crespo NM, et al (2020) Multi-model climate projections of the main cyclogenesis hot-spots and associated winds over the eastern coast of South America. Climate Dynamics 56(1-2):537–557. https: //doi.org/10.1007/s00382-020-05490-1

Dobrynin M, Murawsky J, Yang S (2012) Evolution of the global wind wave climate in CMIP5 experiments. Geophys Res Lett 39(17):2–7. https://doi. org/10.1029/2012GL052843

Fyfe JC (2003) Extratropical Southern Hemisphere cyclones: Harbingers of climate change? J Clim 16(17):2802–2805. https://doi.org/10.1175/ 1520-0442(2003)016h2802:ESHCHOi2.0.CO;2

Gan MA, Rao VB (1991) Surface Cyclogenesis over South America. Mon Weather Rev 119(5):1293–1302. https://doi.org/10.1175/1520-0493(1991) 119h1293:SCOSAi2.0.CO;2

Geng Q, Sugi M (2003) Possible change of extratropical cyclone activity due to enhanced greenhouse gases and sulfate aerosols - Study with a high-resolution AGCM. J Clim 16(13):2262–2274. https://doi.org/10.1175/ 1520-0442(2003)16h2262:PCOECAi2.0.CO;2

Godoi VA, Torres Ju´nior AR (2020) A global analysis of austral summer ocean wave variability during SAM–ENSO phase combinations. Climate Dynamics 54(9-10):3991–4004. https://doi.org/10.1007/s00382-020-05217-2, URL https://doi.org/10.1007/s00382-020-05217-2

Godoi VA, de Andrade FM, Durrant TH, et al (2020) What happens to the ocean surface gravity waves when ENSO and MJO phases combine during the extended boreal winter? Climate Dynamics 54(3-4):1407– 1424. https://doi.org/10.1007/s00382-019-05065-9, URL https://doi.org/ 10.1007/s00382-019-05065-9

Gozzo LF, da Rocha RP, Reboita MS, et al (2014) Subtropical cyclones over the southwestern South Atlantic: Climatological aspects and case study. J Clim 27(22):8543–8562. https://doi.org/10.1175/JCLI-D-14-00149.1

Gozzo LF, da Rocha RP, Gimeno L, et al (2017) Climatology and numerical case study of moisture sources associated with subtropical cyclogenesis over the southwestern Atlantic Ocean. J Geophys Res 122(11):5636–5653. https://doi.org/10.1002/2016JD025764

Gramcianinov CB, Hodges KI, Camargo R (2019) The properties and genesis environments of South Atlantic cyclones. Clim Dyn 53(7-8):4115–4140. https://doi.org/10.1007/s00382-019-04778-1

Gramcianinov CB, Campos RM, de Camargo R, et al (2020a) Analysis of Atlantic extratropical storm tracks characteristics in 41 years of ERA5 and CFSR/CFSv2 databases. Ocean Eng 216:108,111. https://doi.org/10.1016/ j.oceaneng.2020.108111

Gramcianinov CB, Campos RM, de Camargo R, et al (2020b) Atlantic extratropical cyclone tracks in 41 years of ERA5 and CFSR/CFSv2 databases. Mendeley Data V4. https://doi.org/10.17632/kwcvfr52hp.4

Gramcianinov CB, Campos RM, Guedes Soares C, et al (2020c) Extreme waves generated by cyclonic winds in the western portion of the South Atlantic Ocean. Ocean Eng 213(1):107,745. https://doi.org/10.1016/j. oceaneng.2020.107745

Gramcianinov CB, Campos RM, de Camargo R, et al (2021a) Relation between cyclone evolution and fetch associated with extreme wave events in the South Atlantic Ocean. J Offshore Mech Arct Eng 2A-2020:1–27. https://doi.org/ 10.1115/1.4051038

Gramcianinov CB, Campos RM, Guedes Soares C, et al (2021b) Distribution and characteristics of extreme waves generated by extratropical cyclones in the North Atlantic Ocean. In: Guedes Soares C, Santos TA (eds) Developments in Maritime Technology and Engineering. Taylor and Francis, London, UK, p 797–804

Grise KM, Son SW, Gyakum JR (2013) Intraseasonal and interannual variability in north american storm tracks and its relationship to equatorial pacific variability. Mon Weather Rev 141(10):3610–3625. https://doi.org/10.1175/ MWR-D-12-00322.1

Guedes Soares C (1984) Representation of double-peaked sea wave spectra. Ocean Engineering 11(2):185–207. https://doi.org/10.1016/0029-8018(84) 90019-2

Hasselmann K, Barnett TP, Bouws E, et al (1973) Measurements of windwave growth and swell decay during the Joint North Sea wave project (JONSWAP). Deutches Hydrographisches Institut Zeit (A8):1–95

Hemer MA, Church JA, Hunter JR (2010) Variability and trends in the directional wave climate of the southern hemisphere. International Journal of Climatology 30(4):475–491. https://doi.org/10.1002/joc.1900, URL https://doi.org/10.1002/joc.1900

Hersbach H, Bell B, Berrisford P, et al (2020) The ERA5 global reanalysis. Q J R Meteorol Soc 146(730):1999–2049. https://doi.org/10.1002/qj.3803

Hodges KI (1994) A General Method for Tracking Analysis and Its Application to Meteorological Data. Mon Weather Rev 122(11):2573–2586. https://doi. org/10.1175/1520-0493(1994)122h2573:AGMFTAi2.0.CO;2

Hodges KI (1995) Feature Tracking on the Unit Sphere. Mon Weather Rev 123(12):3458–3465. https://doi.org/10.1175/1520-0493(1995)123h3458: FTOTUSi2.0.CO;2

Hodges KI (1996) Spherical Nonparametric Estimators Applied to the UGAMP Model Integration for AMIP. Mon Weather Rev 124(12):2914–2932. https://doi.org/10.1175/1520-0493(1996)124h2914:SNEATTi2.0.CO; 2

Hodges KI (1999) Adaptative Constraints for Feature Tracking. Mon Weather Rev 127:1362–1373. https://doi.org/10.4324/9781315658032

Hodges KI (2008) Confidence intervals and significance tests for spherical data derived from feature tracking. Monthly Weather Review 136(5):1758–1777. https://doi.org/10.1175/2007MWR2299.1

Hoskins BJ, Hodges KI (2002) New Perspectives on the Northern Hemisphere Winter Storm Tracks. J Atmos Sci 59(6):1041–1061. https://doi.org/10. 1175/1520-0469(2002)059h1041:NPOTNHi2.0.CO;2

Hoskins BJ, Hodges KI (2005) A New Perspective on Southern Hemisphere Storm Tracks. J Clim 18(20):4108–4129. https://doi.org/10.1175/JCLI3570. 1, https://arxiv.org/abs/joc.1492 [10.1002]

Hoskins BJ, Hodges KI (2019) The annual cycle of Northern Hemisphere storm tracks. Part I: Seasons. J Clim 32(6):1743–1760. https://doi.org/10.1175/ JCLI-D-17-0870.1

Kita Y, Waseda T, Webb A (2018) Development of waves under explosive cyclones in the Northwestern Pacific. Ocean Dyn 68(10):1403–1418. https: //doi.org/10.1007/s10236-018-1195-z

Lambert SJ, Fyfe JC (2006) Changes in winter cyclone frequencies and strengths simulated in enhanced greenhouse warming experiments: Results from the models participating in the IPCC diagnostic exercise. Clim Dyn 26(7-8):713–728. https://doi.org/10.1007/s00382-006-0110-3

Lemos G, Semedo A, Dobrynin M, et al (2019) Mid-twenty-first century global wave climate projections: Results from a dynamic CMIP5 based ensemble. Glob Planet Change 172:69–87. https://doi.org/10.1016/j.gloplacha.2018. 09.011

Lim EP, Simmonds I (2002) Explosive Cyclone Development in the Southern Hemisphere and a Comparison with Northern Hemisphere Events. Monthly Weather Review 130(9):2188–2209. https://doi.org/10. 1175/1520-0493(2002)130h2188:ecditsi2.0.co;2

Meucci A, Young IR, Hemer M, et al (2020) Projected 21st century changes in extreme wind-wave events. Sci Adv 6(24):eaaz7295. https://doi.org/10. 1126/sciadv.aaz7295

Pezza AB, Ambrizzi T (2003) Variability of Southern Hemisphere Cyclone and Anticyclone Behavior: Further Analysis. J Clim 16:1075–1083. https: //doi.org/10.1175/1520-0442(2003)016h1075:VOSHCAi2.0.CO;2

Ponce de Léon S, Bettencourt J (2021) Composite analysis of North Atlantic extra-tropical cyclone waves from satellite altimetry observations. Adv Sp Res 68(2):762–772. https://doi.org/10.1016/j.asr.2019.07.021

Ponce de Léon S, Guedes Soares C (2014) Extreme wave parameters under North Atlantic extratropical cyclones. Ocean Modelling 81:78–88. https:// doi.org/10.1016/j.ocemod.2014.07.005

Ponce de Léon S, Guedes Soares C (2015) Hindcast of extreme sea states in North Atlantic extratropical storms. Ocean Dynamics 65(2):241–254. https: //doi.org/10.1007/s10236-014-0794-6

Ponce de Léon S, Guedes Soares C (2021) Numerical modelling of the effects of the gulf stream on the wave characteristics. Journal of Marine Science and Engineering 9(1):42. https://doi.org/10.3390/jmse9010042

Rapizo H, Babanin AV, Schulz E, et al (2015) Observation of wind-waves from a moored buoy in the Southern Ocean. Ocean Dyn 65(9-10):1275–1288. https://doi.org/10.1007/s10236-015-0873-3

Reboita MS, da Rocha RP, Ambrizzi T, et al (2015) Trend and teleconnection patterns in the climatology of extratropical cyclones over the Southern Hemisphere. Clim Dyn 45(7-8):1929–1944. https://doi.org/10. 1007/s00382-014-2447-3

Reboita MS, da Rocha RP, de Souza MR, et al (2018) Extratropical cyclones over the southwestern South Atlantic Ocean: HadGEM2-ES and RegCM4 projections. Int J Climatol 38(6):2866–2879. https://doi.org/10.1002/joc. 5468

Reboita MS, Reale M, da Rocha RP, et al (2020) Future changes in the wintertime cyclonic activity over the CORDEX-CORE Southern Hemisphere domains in a multi-model approach. Climate Dynamics 57(5-6):1533– 1549. https://doi.org/10.1007/s00382-020-05317-z, URL https://doi.org/ 10.1007/s00382-020-05317-z

Reboita MS, Crespo NM, Torres JA, et al (2021) Future changes in winter explosive cyclones over the Southern Hemisphere domains from the CORDEX-CORE ensemble. Clim Dyn (1). https://doi.org/10.1007/ s00382-021-05867-w

da Rocha RP, Sugahara S, da Silveira RB (2004) Sea Waves Generated by Extratropical Cyclones in the South Atlantic Ocean: Hindcast and Validation against Altimeter Data. Weather and Forecasting 19(2):398–410. https://doi.org/10.1175/1520-0434(2004)019h0398:swgbeci2.0.co;2

Sanders F, Gyakum JR (1980) Synoptic-dynamic climatology of the "bomb". Monthly Weather Review 108(10):1589–1606. https://doi.org/10.1175/ 1520-0493(1980)108h1589:sdcoti2.0.co;2

Sasaki DK, Gramcianinov CB, Castro B, et al (2021) Intraseasonal variability of ocean surface wind waves in the western south atlantic: the role of cyclones and the pacific south american pattern. Weather and Climate Dynamics 2(4):1149–1166. https://doi.org/10.5194/wcd-2-1149-2021, URL https://doi.org/10.5194/wcd-2-1149-2021

Simmonds I, Keay K (2000) Mean Southern Hemisphere extratropical cyclone behavior in the 40-year NCEP-NCAR reanalysis. J Clim 13(5):873–885. https://doi.org/10.1175/1520-0442(2000)013h0873:MSHECBi2.0.CO;2

Sinclair MR (1994) An objective cyclone climatology for the Southern Hemisphere. https://doi.org/10.1175/1520-0493(1994)122h2239:AOCCFTi 2.0.CO;2

Stopa JE, Cheung KF (2014) Intercomparison of wind and wave data from the ECMWF Reanalysis Interim and the NCEP Climate Forecast System Reanalysis. Ocean Model 75:65–83. https://doi.org/10.1016/j.ocemod.2013. 12.006

Takbash A, Young IR (2020) Long-term and seasonal trends in global wave height extremes derived from ERA-5 reanalysis data. J Mar Sci Eng 8(12):1– 16. https://doi.org/10.3390/jmse8121015

Takbash A, Young IR, Breivik Ø (2019) Global wind speed and wave height extremes derived from long-duration satellite records. J Clim 32(1):109–126. https://doi.org/10.1175/JCLI-D-18-0520.1

Ulbrich U, Leckebusch GC, Pinto JG (2009) Extra-tropical cyclones in the present and future climate: A review. Theor Appl Climatol 96(1-2):117–131. https://doi.org/10.1007/s00704-008-0083-8, https://arxiv.org/abs/9605103 [cs]

Vettor R, Guedes Soares C (2020) A global view on bimodal wave spectra and crossing seas from ERA-interim. Ocean Engineering 210:107,439. https: //doi.org/10.1016/j.oceaneng.2020.107439

Vinoth J, Young IR (2011) Global Estimates of Extreme Wind Speed and Wave Height. J Clim 24(6):1647–1665. https://doi.org/10.1175/2010JCLI3680.1

Wang XL, Swail VR, Zwiers FW (2006) Climatology and changes of extratropical cyclone activity: Comparison of ERA-40 with NCEP-NCAR reanalysis for 1958-2001. J Clim 19(13):3145–3166. https://doi.org/10.1175/JCLI3781. 1

Wang XL, Swail VR, Zwiers FW, et al (2008) Detection of external influence on trends of atmospheric storminess and northern oceans wave heights. Climate Dynamics 32(2-3):189–203. https://doi.org/10.1007/ s00382-008-0442-2, URL https://doi.org/10.1007/s00382-008-0442-2

Young IR (1999) Seasonal variability of the global ocean wind and wave climate. Int J Climatol 19(9):931–950. https://doi.org/10.1002/(SICI) 1097-0088(199907)19:9h931::AID-JOC412i3.0.CO;2-O

Young IR, Ribal A (2019) Multiplatform evaluation of global trends in wind speed and wave height. Science (80-) 364(6440):548–552. https://doi.org/10.1126/science.aav9527

Table 1 Annual mean of cyclones for the different analyzed periods. The climatology values are for all cyclones in the database and associated cyclones indicate only systems related to extreme waves, according to the percentil used to the selection of the wave regions. The percentage for each percentile is calculated in relation to climatology. Values are presented separately for the North Atlantic (NA) and South Atlantic (SA), as well for the DJF and JJA.

Basin & season		period	climatology	number of associated cyclones and percentage		
				90th	95th	99th
NA	DJF	1979-2020	156.0 ± 9.6	38.0 ± 5.1 (24.4%)	25.6 ± 5.1 (16.4%)	9.7 ± 3.1 (6.2%)
		1979-1999	156.3 ± 10.6	37.8 ± 5.0 (24.4%)	25.3 ± 5.0 (16.2%)	10.0 ± 2.7 (6.4%)
		2000-2020	156.0 ± 8.8	38.2 ± 5.3 (24.5%)	25.9 ± 5.2 (16.6%)	9.4 ± 3.6 (6.0%)
	JJA	1979-2020	117.6 ± 8.2	17.5 ± 3.4 (14.9%)	11.2 ± 2.7 (9.5%)	4.9 ± 1.8 (4.2%)
		1979-1999	120.1 ± 7.1	17.6 ± 3.1 (14.6%)	11.0 ± 2.6 (9.1%)	4.8 ± 2.1 (4.0%)
		2000-2020	115.0 ± 3.7	17.5 ± 3.7 (15.2%)	11.4 ± 2.8 (9.9%)	5.0 ± 1.4 (4.4%)
SA	DJF	1979-2020	154.0 ± 9.2	32.5 ± 6.1 (21.1%)	21.1 ± 5.2 (13.7%)	8.3 ± 3.0 (5.4%)
		1979-1999	151.2 ± 8.2	29.6 ± 5.8 (19.6%)	19.8 ± 4.8 (13.1%)	8.1 ± 2.7 (5.4%)
		2000-2020	156.9 ± 9.1	35.3 ± 5.2 (22.3%)	22.4 ± 5.3 (14.3%)	8.5 ± 3.3 (5.4%)
SA	JJA	1979-2020	195.4 ± 10.9	39.2 ± 6.0 (20.0%)	24.4 ± 4.8 (12.5%)	9.2 ± 2.7 (4.7%)
		1979-1999	193.5 ± 9.6	36.3 ± 4.8 (18.8%)	23.4 ± 4.2 (12.1%)	9.5 ± 2.7 (4.9%)
		2000-2020	197.2 ± 12.1	42.0 ± 5.8 (21.3%)	25.4 ± 5.2 (12.9%)	8.8 ± 2.6 (4.5%)

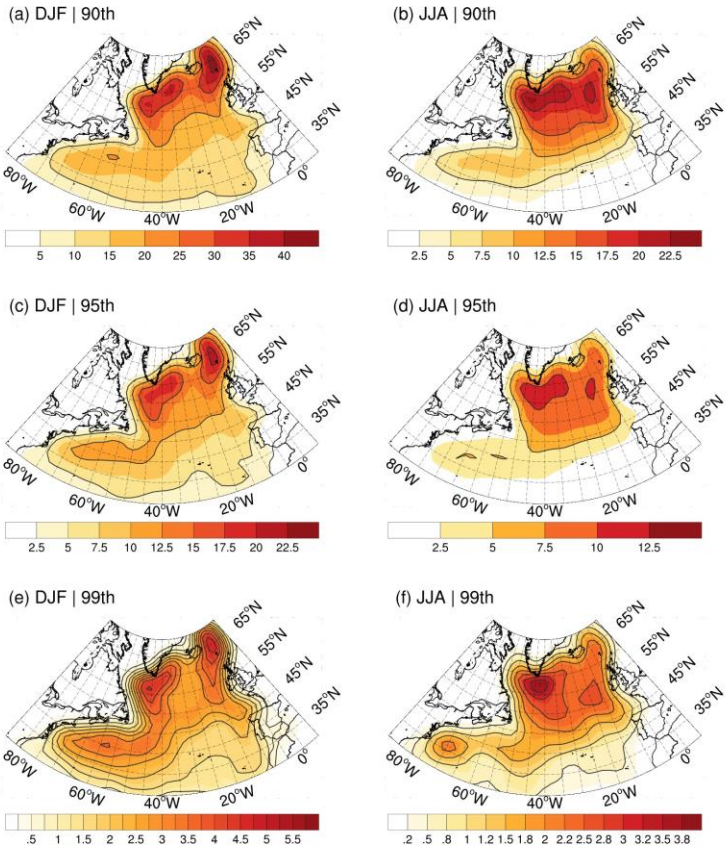

Fig. 1 Density of extreme wave events associated with cyclone (shaded) in the North Atlantic Ocean: in the boreal (a,c) winter (DJF) and (b,d) summer (JJA) for the (a,b) 90^{th}, (c,d) 95^{th}, and (e,f) 99^{th} percentiles of waves events. Density unit is the occurrence of extreme wave regions per month per area, where the area is $10^6 km^2$ ($\sim 5^\circ$ spherical cap). Density is contoured by the double of coloured level intervals.

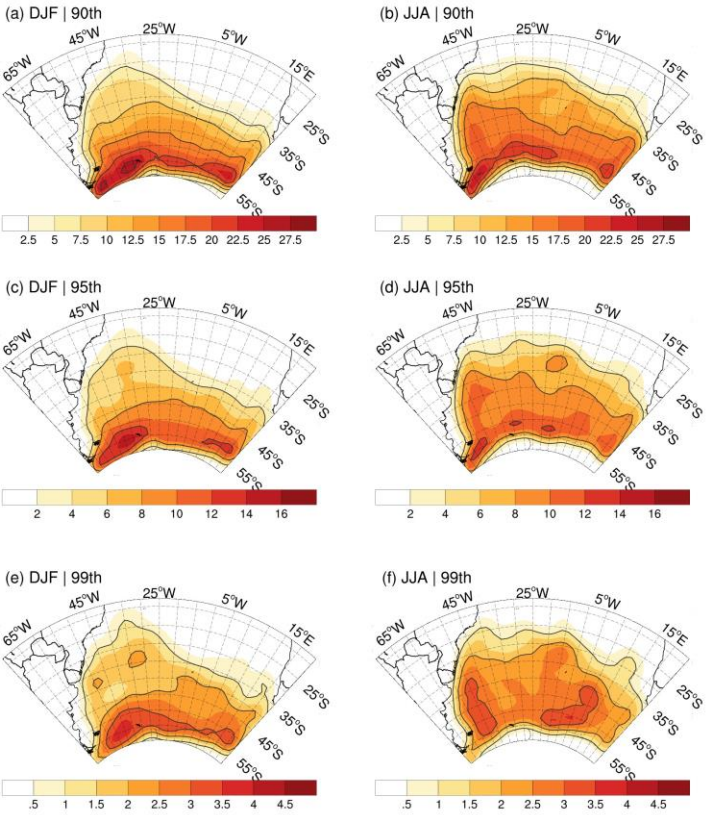

Fig. 2 Density of extreme wave events associated with cyclone (shaded) in the South Atlantic Ocean: in the austral (a,c) summer (DJF) and (b,d) winter (JJA) for the (a,b) 90^{th}, (c,d) 95^{th}, and (e,f) 99^{th} percentiles of waves events. Density unit is the occurrence of extreme wave regions per month per area, where the area is $10^6 km^2$ ($\sim 5^\circ$ spherical cap). Density is contoured by the double of coloured level intervals.

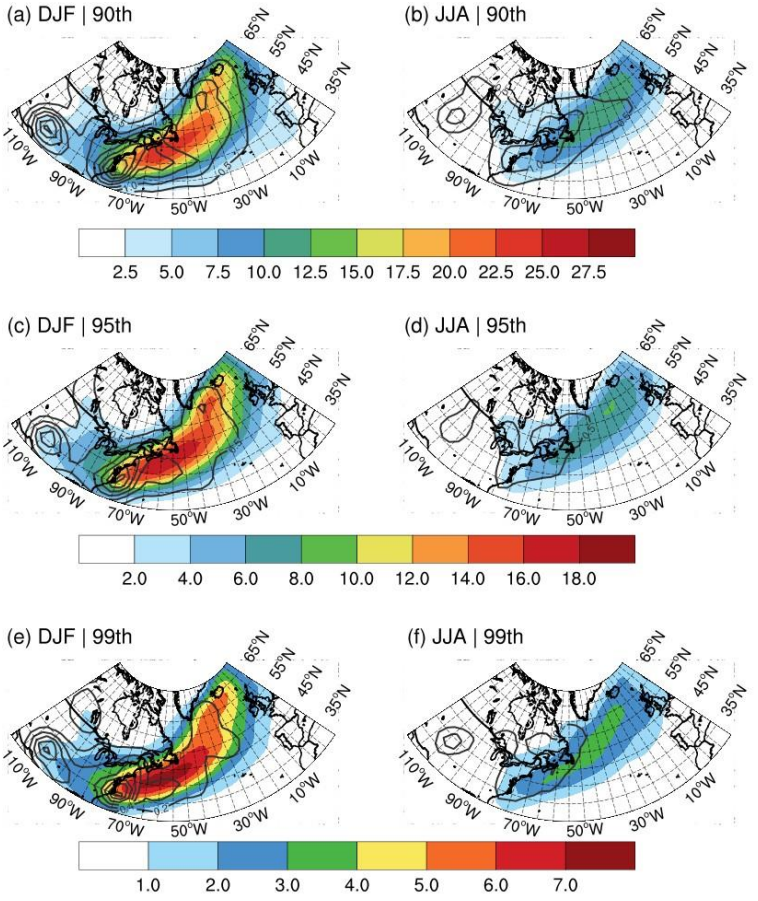

Fig. 3 Cyclone track (shaded) and genesis (contoured) densities associated with extreme waves in the North Atlantic Ocean: in the boreal (a,c,e) winter (DJF) and (b,d,f) summer (JJA) for the (a,b) 90^{th}, (c,d) 95^{th}, and (c,d) 99^{th} percentiles of waves events. Density unit is cyclone per season per area, where the area is $10^6 km^2$ ($\sim 5^\circ$ spherical cap). Cyclogenesis density is contoured by (a-d) 0.5 and (e,f) 0.2 units.

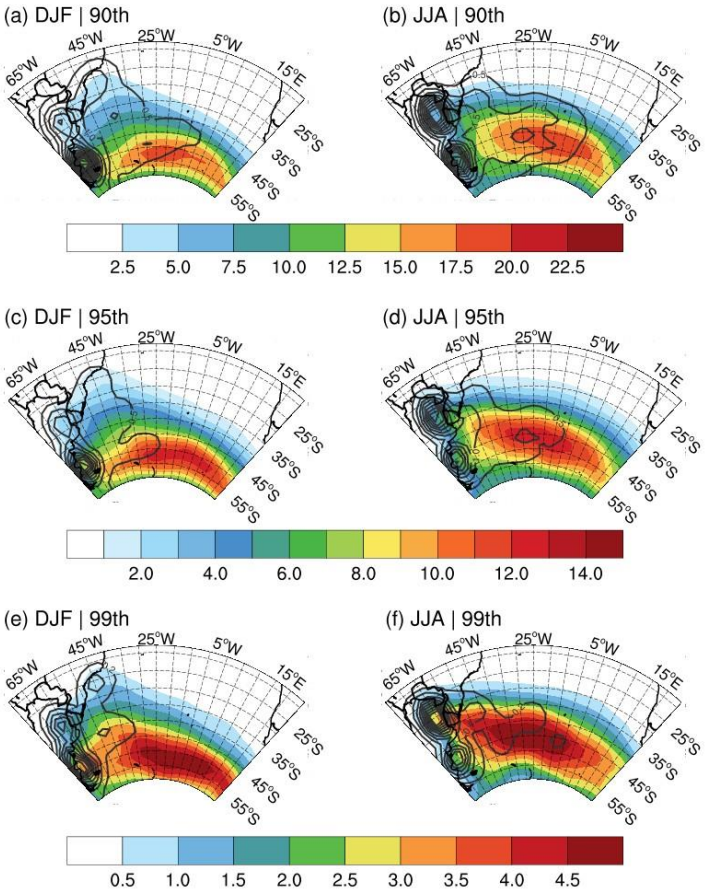

Fig. 4 Cyclone track (shaded) and genesis (contoured) densities associated with extreme waves in the South Atlantic Ocean: in the austral (a,c,e) summer (DJF) and (b,d,f) winter (JJA) for the (a,b) 90^{th}, (c,d) 95^{th}, and (c,d) 99^{th} percentiles of waves events. Density unit is cyclone per season per area, where the area is $10^6 km^2$ ($\sim 5^\circ$ spherical cap). Cyclogenesis density is contoured by (a-d) 0.5 and (e,f) 0.2 units.

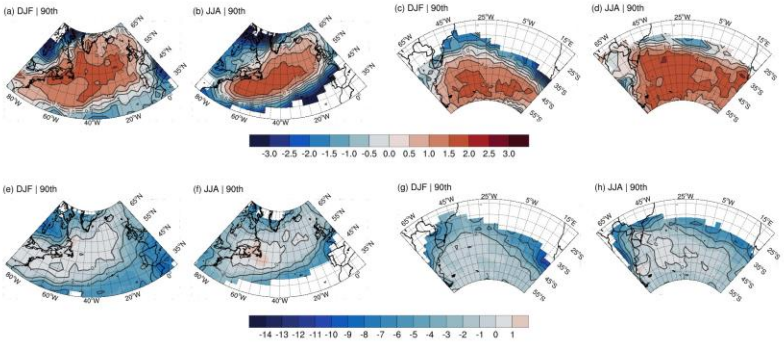

Fig. 5 Differences between cyclone climatology and cyclones associated with extreme waves regarding their (a-d) maximum 10-m winds (m/s) and (e-h) displacement speed (m/s) in the NA (left) and SA (right).

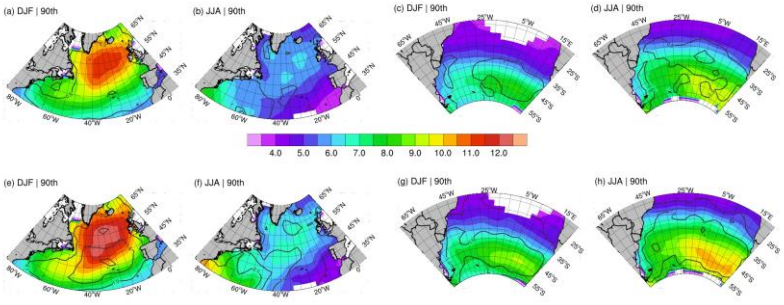

Fig. 6 Distribution maps of (a-d) mean and (e-h) maximum swh (m) of the 90^{th} percentile cyclone-related waves for the NA and SA in the (a,c,e,g) DJF and (b,d,f,h) JJA. The contour lines are the standard deviation in 0.5 intervals.

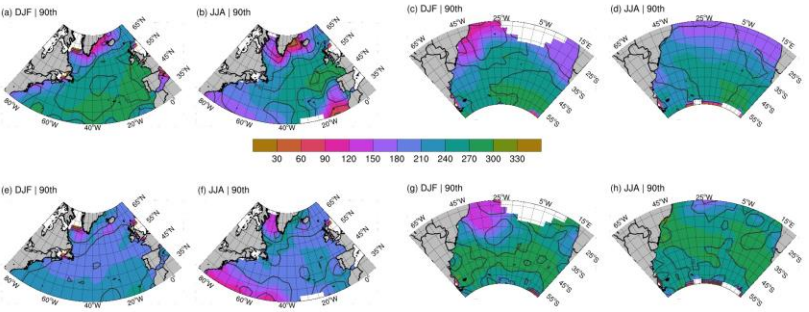

Fig. 7 Distribution maps of (a-d) mean wave direction of the cases and (e-h) cyclone sector where the extreme wave occurred (relative to the center of the cyclone). The contour lines are the standard deviation in 30° intervals. The NA (left) and SA (right) maps are presented in the (a,c,e,g) DJF and (b,d,f,h) JJA considering 90^{th} percentile cyclone-related waves.

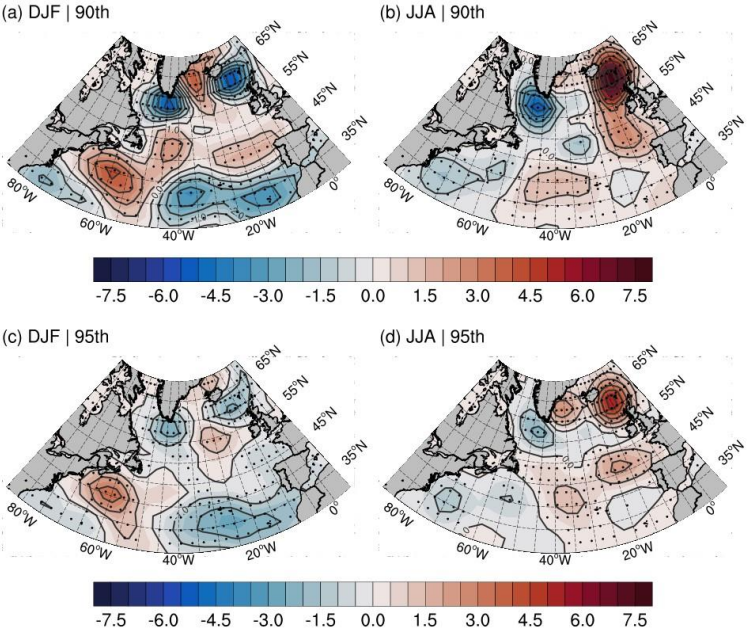

Fig. 8 Changes in the cyclone-related wave occurrence in the North Atlantic based on the (a,b) 90^{th} and (c,d) 95^{th} percentiles for the (a,c) DJF and (b,d) JJA. Changes are computed based on the difference between 2020-2000 and 1979-1999 periods. Significant differences (p-value < 0.1, t-test) are marked with black dots.

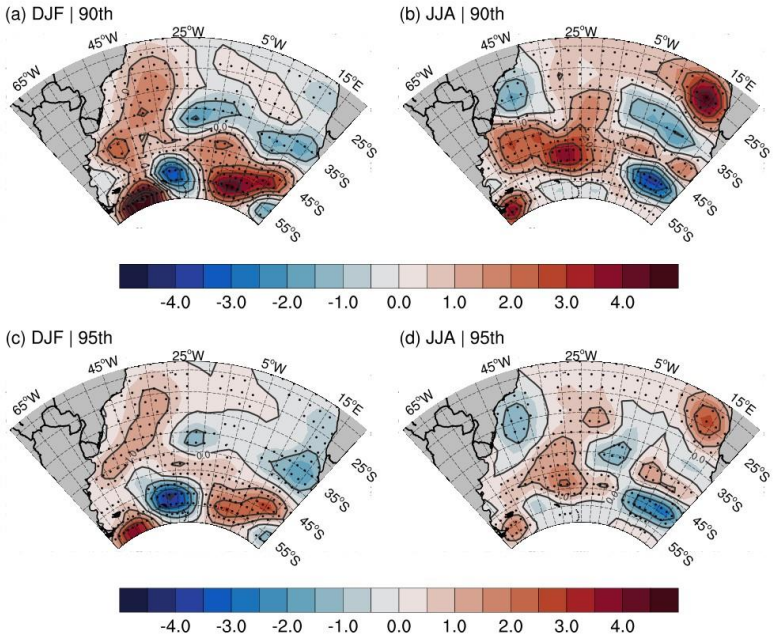

Fig. 9 Changes in the cyclone-related wave occurrence in the South Atlantic based on the (a,b) 90^{th} and (c,d) 95^{th} percentiles for the (a,c) DJF and (b,d) JJA. Changes are computed based on the difference between 2020-2000 and 1979-1999 periods. Significant differences (p-value < 0.1, t-test) are marked with black dots.

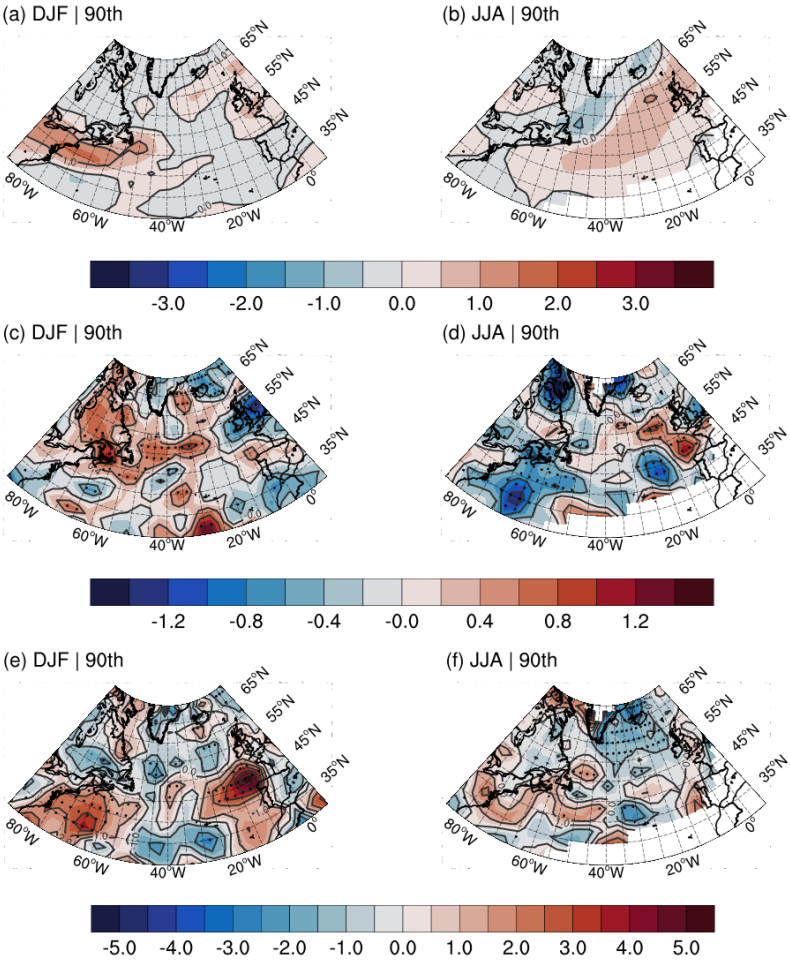

Fig. 10 Changes in the North Atlantic cyclone (a,b) track density (tracks per season per $10^6 km^2$), (c,d) vorticity at 850 hPa ($10^5 s^{-1}$), and speed (m/s) in the (a,c,e) DJF and (b,d,f) JJA related to the 90^{th} percentile. Significant differences (p-value < 0.1) are marked with black dots. Regions with track density smaller than 0.3 cyclones per season are not plotted. Black contoured lines have the double of shaded intervals.

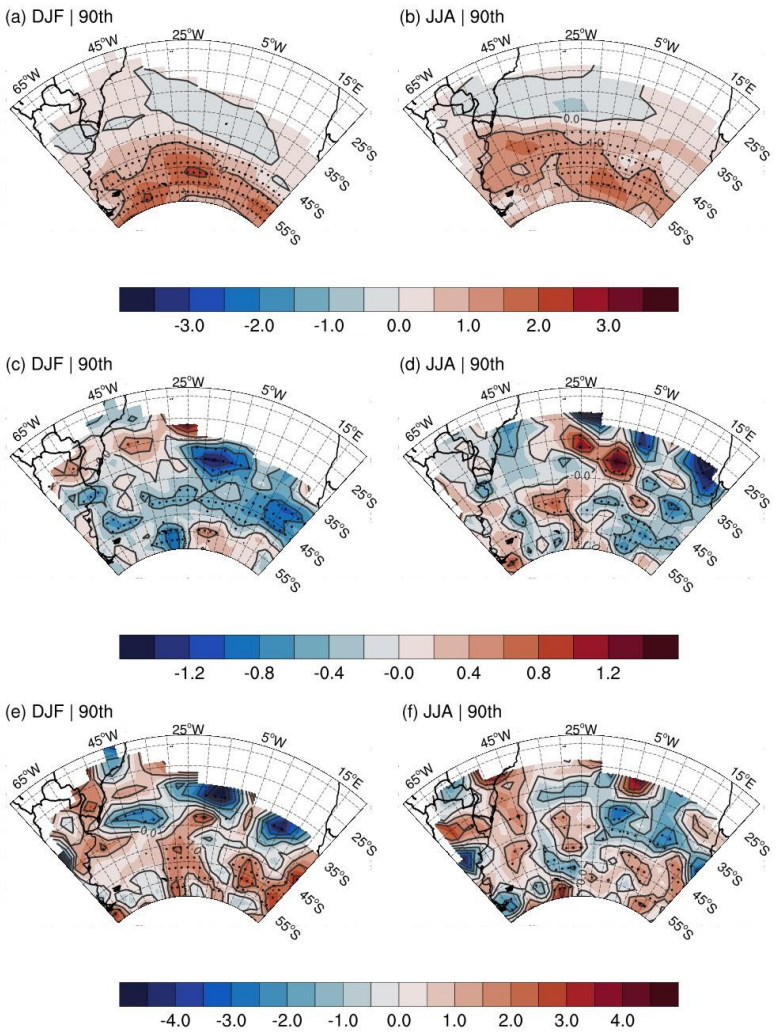

Fig. 11 Changes in the South Atlantic cyclone (a,b) track density (tracks per season per $10^6 km^2$), (c,d) vorticity at 850 hPa ($10^5 s^{-1}$), and speed (m/s) in the (a,c,e) DJF and (b,d,f) JJA related to the 90^{th} percentile. Significant differences (p-value < 0.1) are marked with black dots. Regions with track density smaller than 0.3 cyclones per season are not plotted. Black contoured lines have the double of shaded intervals.

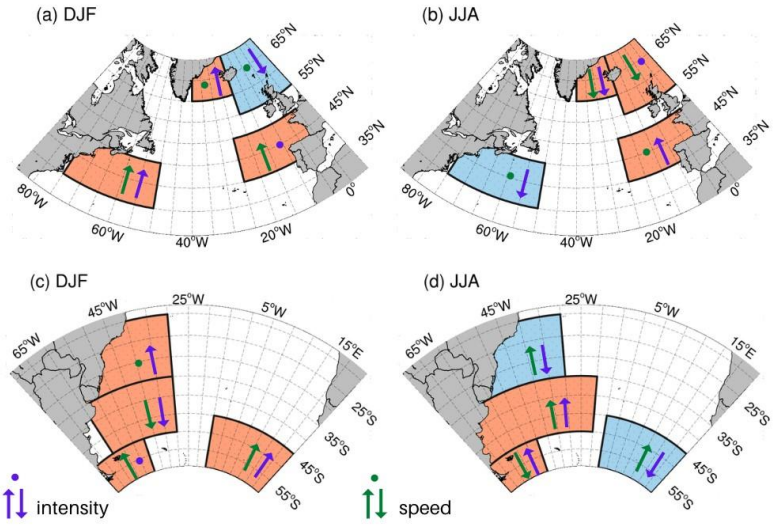

Fig. 12 Summary scheme of changes in the (a,b) North and (c,d) Atlantic cyclone-related extreme waves in present climate and their main driving mechanisms regarding storm track characteristics. The hot-spots are defined by back boxes filled with light red and blue for increase and decrease of extreme wave occurrence, respectively. Upward (downward) arrows indicate increase (decrease) of cyclone intensity (purple) and displacement speed (green) while the dots show non-significant signal.

Appendix A: Supplementary Material

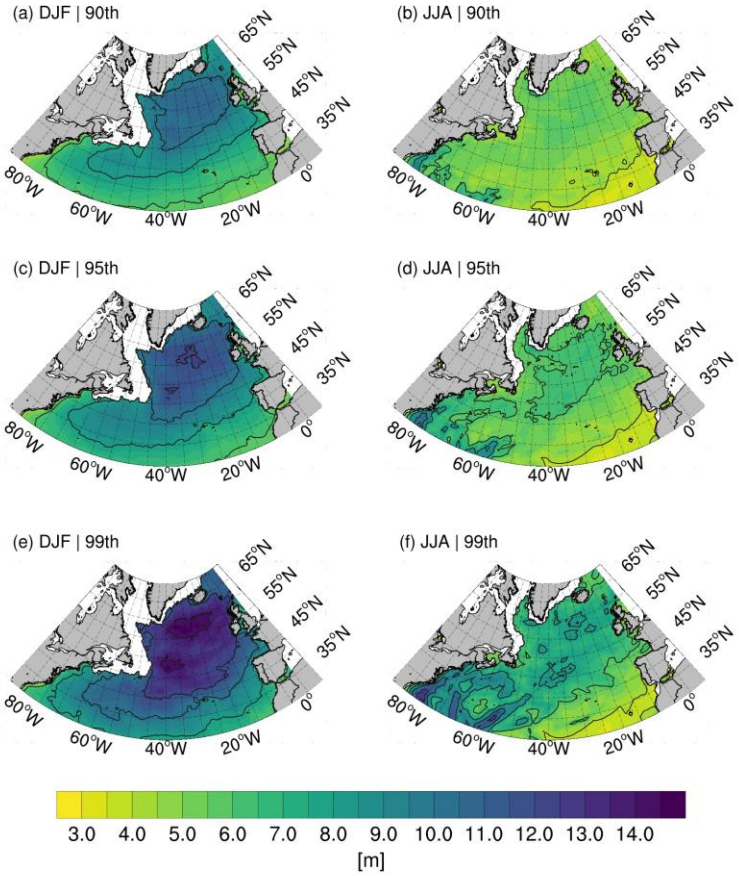

Fig. A1 The swh thresholds obtained based on the (a,b) 90th, (c,d) 95th, and (e,f) 99th percentiles for the North Atlantic basins in the (a,c,e) DJF and (b,d,f) JJA. Black contours are in 2 m intervals.

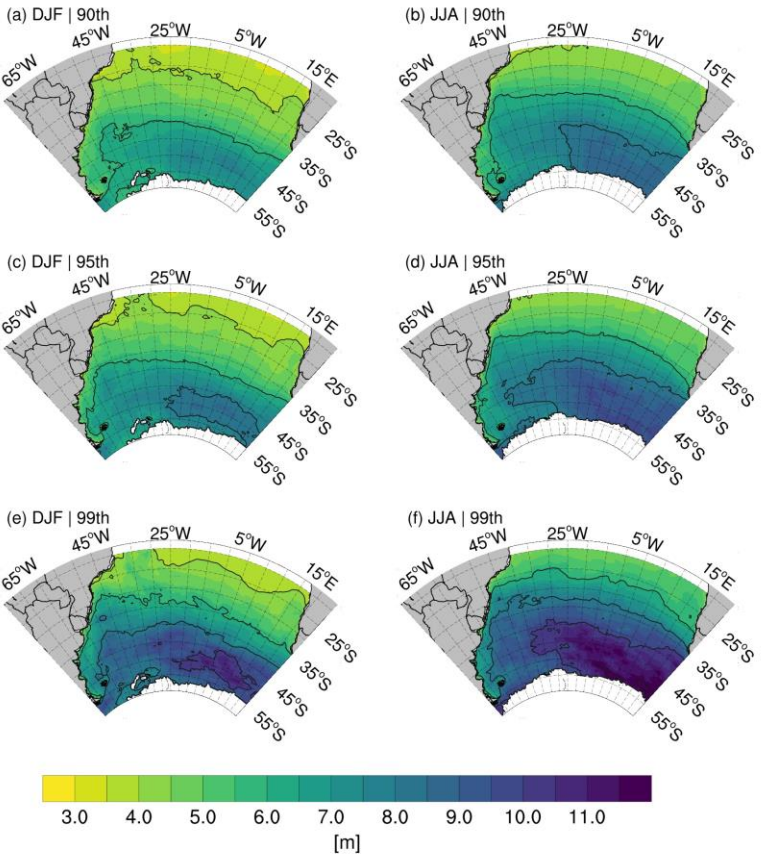

Fig. A2 The swh thresholds obtained based on the (a,b) 90^{th}, (c,d) 95^{th}, and (e,f) 99^{th} percentiles for the South Atlantic basins in the (a,c,e) DJF and (b,d,f) JJA. Black contours are in 2 m intervals.

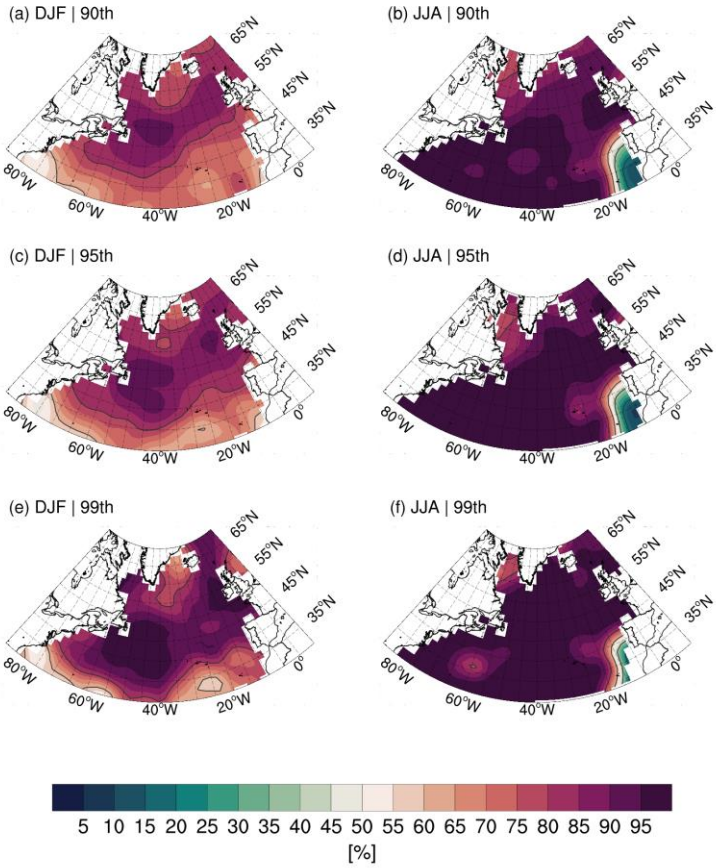

Fig. A3 The percentage of extreme wave events associated with cyclones in the all extreme waves above the (a,b) 90th, (c,d) 95th, and (e,f) 99th–percentile swh for the North Atlantic basin in the (a,c,e) DJF and (b,d,f) JJA. Black contours are in 20% intervals.

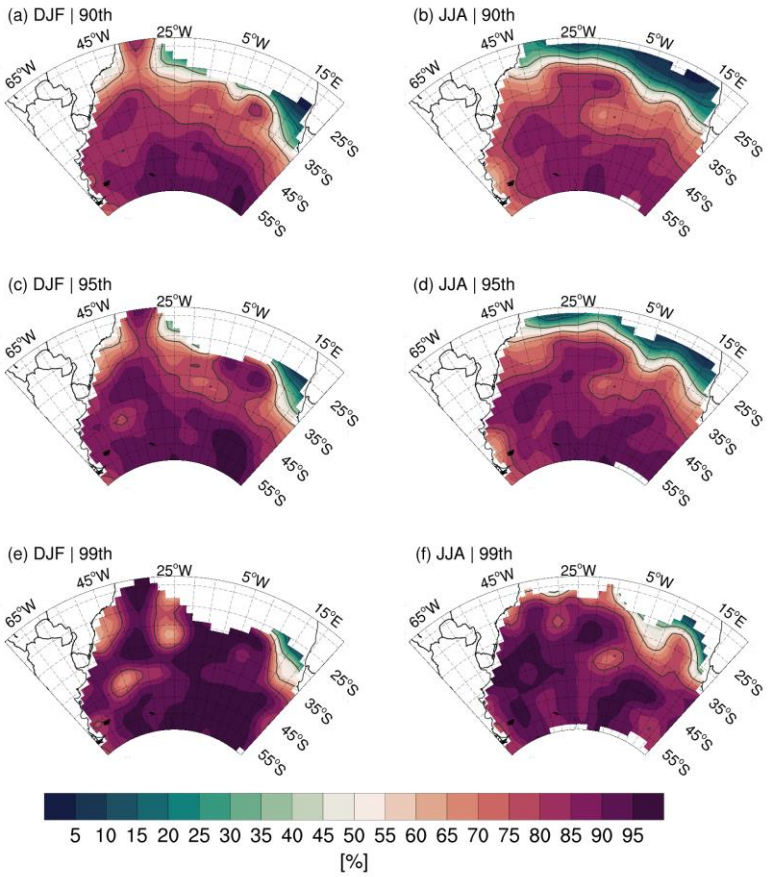

Fig. A4 The percentage of extreme wave events associated with cyclones in the all extreme waves above the (a,b) 90^{th}, (c,d) 95^{th}, and (e,f) 99^{th}–percentile swh for the South Atlantic basin in the (a,c,e) DJF and (b,d,f) JJA. Black contours are in 20% intervals.

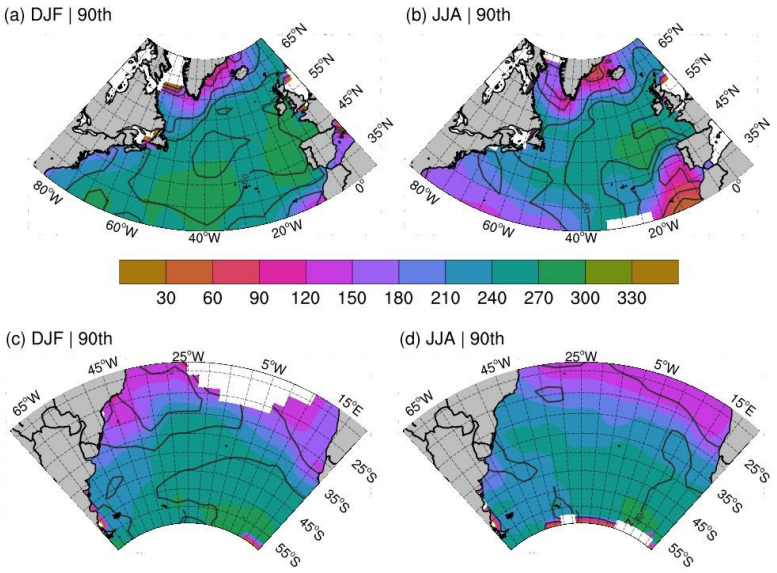

Fig. A5 Distribution maps of the mean 10-m wind direction of the 90^{th} cases for the (a,b) NA and (c,d) SA in the (a,c) DJF and (b,d) JJA. The contour lines are the standard deviation in 30° intervals.